

GT2020-14498

THERMODYNAMIC AND MECHANICAL DESIGN CONCEPT FOR MICRO-TURBOJET TO MICRO-TURBOSHAFT ENGINE CONVERSION

Christoph Öttl, Reinhard Willinger

Institute of Energy Systems and Thermodynamics
Technische Universität Wien
Getreidemarkt 9/302, A-1060 Vienna, Austria
christoph.oettl@tuwien.ac.at
reinhard.willinger@tuwien.ac.at

ABSTRACT

In this work, a design concept for micro-turbojet to micro-turboshaft engine conversion is presented. This is motivated by a lack of available micro-turboshaft engines which is shown in the market survey conducted. Thus, the presented concept deals with the conversion of an existing micro-turbojet engine to a micro-turboshaft engine for a specific power output. The conversion is shown using the micro-turbojet engine OLYMPUS HP from AMT Netherlands. Furthermore, the simultaneously developed analytical preliminary design of the additional single-stage power turbine is shown besides a thermodynamic cycle simulation. This has been done to obtain the unknown gas generator outlet condition which is similar to the power turbine's inlet condition. Within the cycle calculation, occurring losses due to the small dimensions have also been considered. During the design process, different combinations of work coefficient and mean diameter of the power turbine were investigated to minimize the required gear box ratio for a given rotor speed in terms of weight minimization. To keep losses in the power turbine low, the preliminary blade row has finally been improved using CFD calculations.

NOMENCLATURE

a specific work
 A flow area
 b axial chord length

c absolute velocity
 d diameter
 F thrust
 h specific enthalpy
 H_U heating value
 l blade length
 \dot{m} mass flow rate
 Ma Mach number
 p pressure
 P power
 R_k degree of reaction
 Re Reynolds number
 t blade pitch
 T temperature
 u circumferential velocity
 w relative velocity
 y^+ dimensionless wall distance
 α absolute flow angle
 β relative flow angle
 η efficiency
 λ work coefficient
 φ flow coefficient
 Π pressure ratio
 Ψ Zweifel coefficient
 ρ density
 ω total pressure loss coefficient

Subscripts

4	gas generator turbine stator inlet
5	gas generator turbine rotor inlet
6	gas generator turbine rotor outlet
7	power turbine stator inlet
8	power turbine rotor inlet
9	power turbine rotor outlet
10	nozzle exit
<i>B</i>	blade
<i>C</i>	compressor
<i>in</i>	initial
<i>ex</i>	extended
<i>GG</i>	gas generator
<i>m</i>	mean
<i>P</i>	propeller
<i>PT</i>	power turbine
<i>s</i>	isentropic
<i>t</i>	total
<i>T</i>	turbine
<i>u</i>	circumferential
<i>z</i>	axial direction

Superscripts

*	initial guess
—	mass averaged quantity

Abbreviations

CFD	computational fluid dynamics
EGT	exhaust gas temperature
GGT	gas generator turbine
ITD	intermediate turbine duct
UAV	unmanned aerial vehicle

INTRODUCTION

During the last years, the demand of unmanned aerial vehicles (UAV) for private and commercial use has grown very rapidly. Various technologies can be used to power an UAV: electric motor, internal combustion engine, gas turbine. Each technology has its specific advantages and disadvantages. The gas turbine shows a favourable behaviour of torque over rotational speed as well as lower vibrations in comparison to internal combustion engines for example. Otherwise, the high weight of an electric motor and its battery is a disadvantage for any aircraft application. Because the trend is towards higher maximum take-off weights (MTOW), the required drive power increases. Furthermore, shaft power is needed for drone propulsion. The presented engine design concept was created for the requirements of a single copter drone in hover flight. For a given MTOW of 25 kg, a power demand between 20 and 40 kW depending on the propeller design is estimated. This design is not exactly known

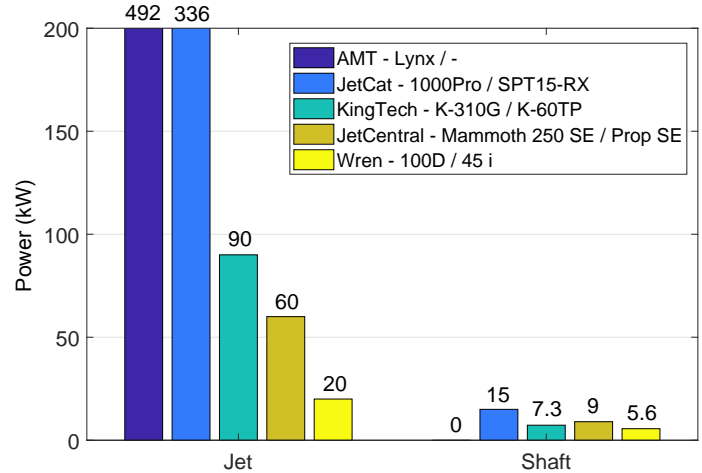


FIGURE 1. MAXIMUM AVAILABLE DRIVE POWER OF MICRO-TURBOJET AND MICRO-TURBOSHAFT ENGINES

at this time, but the propeller diameter is about 0.7 m. A preliminary market survey has shown, that there are no turboshaft engines available above 15 kW, but jet engines for higher equivalent power ranges can be obtained though (Fig. 1, also see [1]). To reduce the design effort, an existing jet engine can therefore be used as the basis of a new turboshaft engine [1] with an output of more than 15 kW. The existing turbojet engine serves as a gas generator for the turboshaft engine, whereby an intermediate turbine duct (ITD) replaces the jet nozzle and connects the gas generator turbine with the power turbine. In addition to the existing gas generator turbine, only the power turbine has to be designed. Due to the simple design of these low power range engines, the designing part of the conversion is relatively easy to realize and the existing gas generator easy to integrate. There have already conversions been conducted using the micro-turbojet engines JetCat-P200 [2] and Wren100 [3]. In this paper, data from the Olympus HP engine from AMT Netherlands were used for the conversion [4]. A cross section of this engine is shown in Fig. 2. Since AMT offers an "University configuration", several works depending this engine have already been published [5–9]. Bakalis and Stamatis [7] already published a model calibration for educational purpose concerning this engine. A wide range of performance data of the Olympus HP under transient operating conditions was also published by Leyelek et al. [5] and Leyelek [6], as well as by Rahman and Whidborne [8], based on experimental investigations and numerical calculations.

The present design concept is limited to operation at constant rotor speed. As with helicopters, it is obvious that drones with gas turbine propulsion also have to be operated at constant rotor speed. In addition, only design point data is provided by the manufacturer. Because of this lack of information, component efficiencies and losses of the gas generator have to be estimated in order to determine the boundary conditions of the power

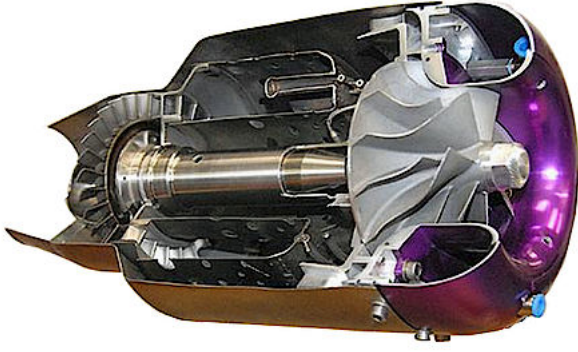


FIGURE 2. AMT OLYMPUS HP [12]

TABLE 1. OLYMPUS HP SPECIFICATIONS [4]

Specifications	
Thrust [N]	230
Rotational speed [rpm]	108500
Compressor pressure ratio [-]	3.8
Air mass flow rate [kg/s]	0.45
Exhaust gas temperature (max) [°C]	700 (750)
Fuel consumption [kg/s]	0.01

turbine. Therefore, a thermodynamic cycle model was developed with the commercial software IPSEpro. Since the model is designed for micro engines, additional losses due to heat transfer [10] leading to non-adiabatic compression [11] occur, which have been considered. Furthermore it is desirable, that the power turbine's mean diameter is as large as possible to keep the propeller shaft speed in a low range. For a given work coefficient, the turbine speed reduces as the mean diameter increases. Due to the high speeds of the gas generator shaft, however, it is not possible to achieve sufficient speed reduction simply by increasing the power turbine's mean diameter. This is because the propeller shaft speed of the prototype drone is designed to run at 5000 rpm, while the gas generator shaft runs at 108500 rpm at the design point according to AMTs specifications (Tab. 1). The speed of the free running power turbine is about half of the gas generator shaft speed (Tab. 5). It is therefore necessary to provide an additional reduction gear between the power shaft and the propeller shaft. Therefore, different combinations of work coefficient and turbine mean diameter were examined to determine the combination leading to the lowest gear ratio in order to minimize gear box weight. Beside weight reduction, there are no restrictions depending the reduction gear box at first.

POWER ESTIMATION

In the first step of the conversion, an appropriate jet engine has to be chosen. Since jet engines are usually characterized by Thrust F and mass flow rate \dot{m} , an equivalent power value must be calculated to estimate how much shaft power can be generated using a particular jet engine. According to the ideal turbojet cycle (Fig. 3), the kinetic energy $c_{10}^2/2$ represents the available amount of energy which can be converted into shaft power. Thrust can be calculated using the equation of linear momentum, as can be seen in Eqn. (1).

$$F = \dot{m}(c_{10} - c_0) \quad (1)$$

Since the inlet velocity c_0 equals 0 in case of hovering and $c_0 \ll c_{10}$ in case of vertical lift, one can neglect c_0 in Eqn. (1). Furthermore, an equivalent power value based on the kinetic energy, can be calculated with

$$P = \dot{m} \frac{c_{10}^2}{2} \quad (2)$$

Through combination of Eqn. (1) and (2), the available power can finally be obtained using only the given values F and \dot{m} , as shown in Eqn. (3).

$$P = \frac{F^2}{2\dot{m}} \quad (3)$$

The power estimation for the AMT Olympus HP according to

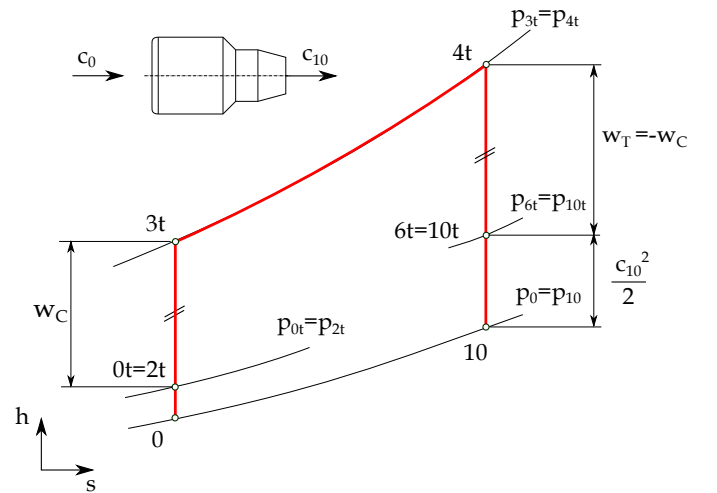


FIGURE 3. IDEAL TURBO JET CYCLE

Eqn. (3) leads to a convertible shaft power of 58.8 kW. The engine specifications given by AMT Netherlands can be seen in Tab. 1.

THERMODYNAMIC CYCLE MODEL

According to the chosen jet engine Olympus HP, an appropriate cycle model has been created with the software IPSEpro. A first simplified model is shown in Fig. 4. Therefore, the existing jet engine, which serves as gas generator (GG), has been extended by a free running power turbine (PT). As the given compressor pressure ratio Π_C is defined as a static-to-static value according to AMT, the cycle calculation has been carried out with static values neglecting any pressure losses. Ambient conditions have to be defined at the compressor inlet as well as the ambient pressure at the PT-outlet. Due to the mentioned flight conditions, standard temperature and pressure (STP) have been defined. Unknown component efficiencies have to be estimated as good as possible at first and the heating value has to be defined according to the used propellant. Since the given engine specifications are valid under the usage of Kerosene Jet A-1, the heating value must correspond to this propellant and was therefore set to $H_U=42800$ kJ/kg. First results under consideration of the given engine specifications show, that especially the turbine outlet temperature deviates strongly from the specified value (Initial model in Tab. 2). Because the turbine outlet conditions are most important for the conversion as the gas generator turbine outlet conditions are similar to the power turbine's inlet conditions, the model has been extended by several modifications to meet the given values (Fig. 5). The aim is to map the selected engine in the best possible way, to limit the unknown parameters as far as possible. First of all, the compressor pressure ratio has been reduced to consider non adiabatic compression [11], since inlet air is pre-heated due to the small dimensions. Since [5] and [7] both have measured a pressure ratio of 3.5 against the given value of 3.8 from AMT at the design point, it can be assumed that the non-adiabatic compression can be taken into account by reducing the

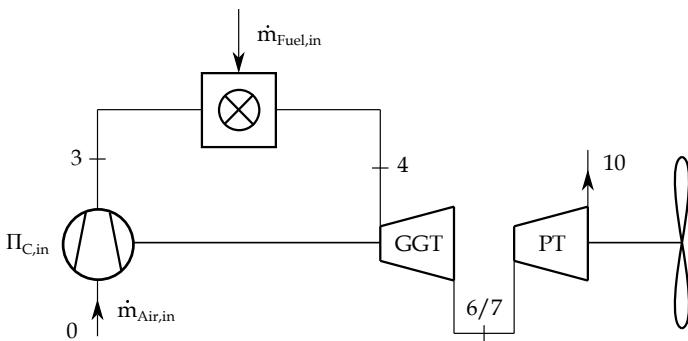


FIGURE 4. INITIAL CYCLE MODEL

pressure ratio by approximately 8 % (Eqn. (4)).

$$\Pi_{C,ex} = 0.92 \cdot \Pi_{C,in} \quad (4)$$

Furthermore, the air mass flow specified by AMT was increased by 10 % according to [6] (Eqn. (5)).

$$\dot{m}_{Air,ex} = 1.1 \cdot \dot{m}_{Air,in} \quad (5)$$

The given fuel mass flow rate has also been reduced by 11 % , to meet an appropriate EGT at the turbine outlet according to the measurements of [5] as listed in Tab. 2. This leads to a fuel mass flow according to Eqn. (6).

$$\dot{m}_{Fuel,ex} = 0.89 \cdot \dot{m}_{Fuel,in} \quad (6)$$

As [5] also describes, fuel mass flow given by AMT is measured directly at the fuel tank exit and includes fuel for lubrication. To consider this, the fuel mass flow which is defined at the combustion chamber inlet has to be reduced in the present model. Furthermore, a heat loss through the engine housing was taken into account. A value of 3 kW was considered in a first rough estimation for static heat transfer. By varying heat loss between 0 and 3 kW it turns out, that heat loss has only a minor effect on the EGT in this range. In addition, disc and shroud cooling have been considered as shown in Fig. 6. According to Rodgers [14], it is not possible to provide internal rotor cooling passage because of the small dimensions of micro-turbines. Depending on the GGT inlet temperature, an air mass flow rate of 2% for disc cooling purpose is assumed [14]. This mass flow rate does not take part at the combustion and is mixed into the hot gas stream at the turbine inlet. It is also assumed, that another 3% of the air mass flow

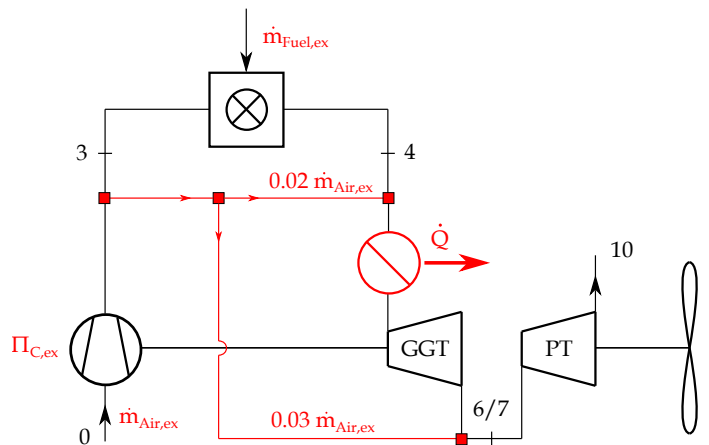


FIGURE 5. EXTENDED CYCLE MODEL

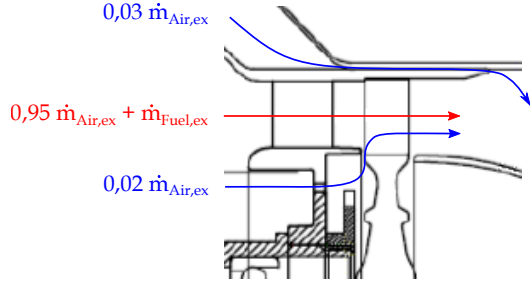


FIGURE 6. TURBINE COOLING AIR MASS FLOW [13]

rate does not take part at the expansion through the turbine and is mixed into the gas stream at the turbine outlet instead. This is done for the purpose of shroud cooling. This method is a common way of cooling within micro-turbomachinery. All these considerations lead to a reduced EGT by using the extended model. The comparison of the results are shown in Tab. 2. Due to lack of information, compressor and turbine efficiencies have been estimated with $\eta_{sC}=0.74$ and $\eta_{sT}=0.92$. In accordance with [9] ($\eta_{sC}=0.72$ and $\eta_{sT}=0.85$), the chosen efficiencies represent a good approximation since the developed model from Vannoy and Cadou fits the measurements quite well. Turbine efficiency is slightly higher than in [9] but is however further reduced due to the considered amount of air mass flow, which is not taking part on the expansion. Furthermore, [2] uses a turbine efficiency of 0.89 for a comparable engine (JetCat P200, $F=230$ N, $\Pi_C=3.7$, $\dot{m}_{Air}=0.45$ kg/s). Comparing the obtained EGTs, there is a good agreement between the extended model and the given values. To make the EGTs comparable, the static temperature gained from the modelling was converted into total temperature. Also, the measured value from [5] has been extrapolated to the maximum shaft speed ($n=108500$ rpm) of the GG, since temperature is only provided at $n=105700$ rpm. Furthermore, the extended model shows significant improvement over the initial model. It can therefore be assumed that all these factors must be taken into account in the modelling. A scheme of the final extended model

TABLE 2. COMPARISON OF SPECIFIED AND CALCULATED EGTs WITH DIFFERENT MODELS

Model / Exp.	EGT [°C]
AMT specifications (max)	700 (750) $\pm 2\%$
Exp. Leylek [5]	754
Initial model	908
Extended model	752

is shown in Fig. 5. Additionally, heat and frictions losses will probably occur at the ITD and can easily be adapted. Since the final dimensions of the ITD are not known at this time, this heat loss has not been taken into account for this model. In addition to the adequate EGT, the extended model calculates a shaft power of about 60 kW (without mechanical losses), which is in good agreement with the estimated power of 58.8 kW according to Eqn. (3).

FLOW CONDITIONS

Gas generator turbine

Figure 7 shows the single stage axial turbine of the GG. While pressure p , density ρ and temperature T at the turbine's inlet and outlet (section 4 and 6) have been gained through the thermodynamic cycle calculation, flow velocities have not been considered yet. However, this is necessary for the power turbine design. Therefore, at least the mean diameter d_m and blade lengths l_4 and l_6 , hence the flow areas A_4 and A_6 have to be known. For the given engine, the dimensions are $d_m=73$ mm, $l_4=10$ mm and $l_6=12$ mm. According to the balance of mass, the guide vane inlet velocity c_4 can then be calculated with

$$c_{i,z} = \frac{\dot{m}_{Air,ex} + \dot{m}_{Fuel,ex}}{\rho_i \cdot d_m \cdot \pi \cdot l_i} \Bigg|_{i=4,5,6} \quad (7)$$

Due to lack of information, swirl free inflow has been assumed ($c_4 = c_{4,z}$ and $\alpha_4 = 90^\circ$). It is also to be assumed, that the turbine is designed in a way, where the absolute turbine outlet velocity is also widely without swirl ($c_6 = c_{6,z}$ and $\alpha_6 = 90^\circ$). This is because thrust is as high as possible in this case for a specified velocity. Under this assumption, the absolute velocity c_6 can also be obtained with the balance of mass according to Eqn. (7). To support the assumption, a mean line analysis has been carried out. Therefore an iterative loop using MATHCAD has been created as shown in Fig. 8. With the gained enthalpies h_4 and h_6 from the thermodynamic cycle calculation and the pre-calculated velocities c_4 and c_6 , one can calculate the absolute and relative velocities at section 5, whereby the degree of reaction R_k and the absolute flow angle α_5 must also be estimated with an initial guess at first. Therefore, common values for reaction stages according to Tab. 3 can be used.

TABLE 3. GUIDELINE VALUES FOR REACTION STAGES

R_k [-]	α_5 [°]	β_6 [°]
0,5	14-40	140-160

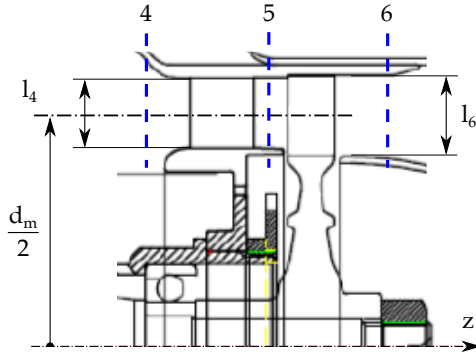


FIGURE 7. AMT OLYMPUS HP GG-TURBINE [13]

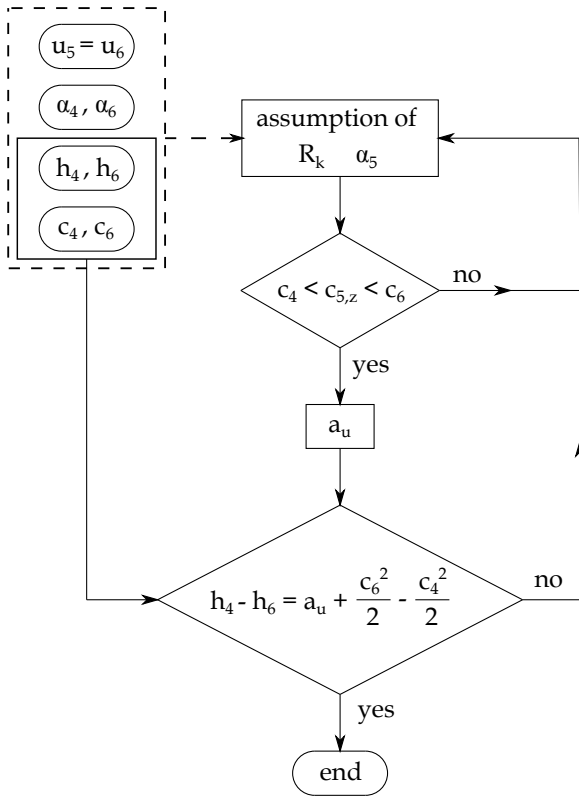


FIGURE 8. GG-TURBINE FLOW CHART

Finally the specific work and the power of the turbine can be calculated respectively. This value can now be compared with the gained value from the thermodynamic cycle calculation. In case of good agreement, the calculation is finished and it can be assumed, that swirl-free outflow represents an optimal flow condition conventionally sought. The results for the chosen engine are shown in Tab. 4. Flow coefficient $\varphi = c_{5m}/u_m = 0.68$, work coefficient $\lambda = a_u/u_m^2 = 0.97$ and degree of reaction $R_k = 0.52$

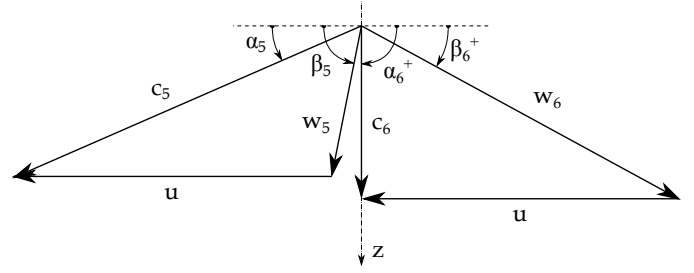


FIGURE 9. VELOCITY TRIANGLE GG-TURBINE

take conventional values. This also indicates, that the assumed values correspond quite well to the real engine. Figure 9 shows the velocity triangles of the turbine stage. The cross-sectional expansion over the stage is too weak to ensure constant meridional velocity c_z for the dominant decrease of density. It is therefore obvious that the meridional velocity increases.

TABLE 4. GG-TURBINE FLOW CONDITIONS

Section	4	5	6
h [kJ/kg]	1005	906	799
c [m/s]	205	490	297
c_z [m/s]	205	281	297

POWER TURBINE DESIGN

Main dimensions

To design the power turbine, another iteration loop has been developed to obtain the main dimensions of the turbine via mean line analysis (Fig. 10). Besides the calculation of the flow velocities, the conservations of energy and mass have to be fulfilled. Power P_P and speed n_P of the propeller shaft are given and depend on the mentioned UAV requirements. Furthermore, mass flow rate is given and optimal swirl free outlet flow ($\alpha_9 = 90^\circ$) is assumed. Work coefficient λ_{PT} , mean diameter $d_{m,PT}$ and blade height l_{PT}^* must be chosen initially. Then, a required gearbox ratio i can already be calculated. As a guideline for the initial guess, the following limitations have been specified:

- $1 \leq \lambda_{PT} \leq 2$
- $\alpha_8 \leq 40^\circ$
- $d_{m,PT,max} = 2 \cdot d_{m,GG}$
- $l_{PT} \leq l_{GG}$

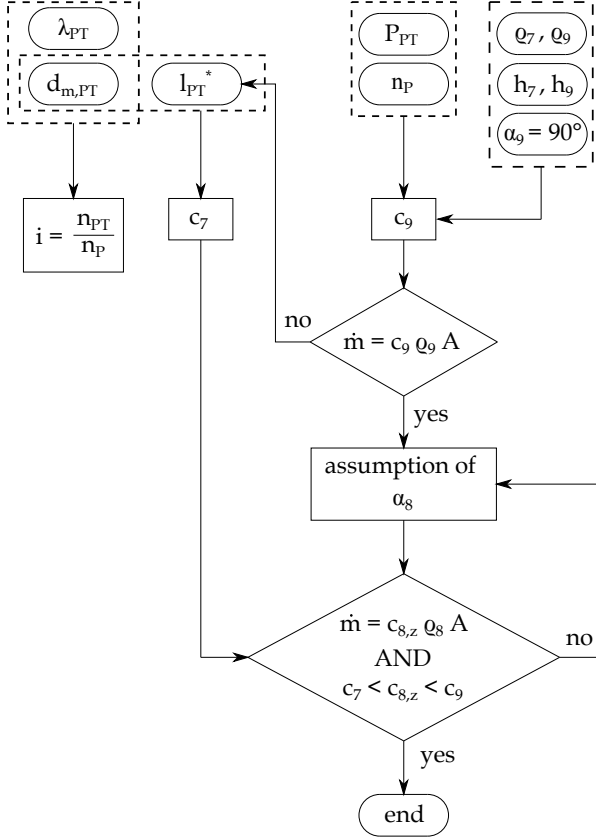


FIGURE 10. PT-TURBINE DESIGN FLOW CHART

With the energy conservation and the gained boundary conditions from the cycle calculation, the absolute outlet velocity c_9 can be obtained. Using the calculated velocity, the mass flow rate must correspond to the given value to meet the mass balance. If the values do not agree, the blade height has to be changed. It should be mentioned, that the blade height has been chosen to be constant over the whole stage. As already shown for the GG-turbine, the absolute flow angle α_8 has to be chosen to meet the mass conservation in section 8. While the cycle calculation only provides values at section 7 and 9, density at guide vane outlet has been calculated under assumption of isentropic expansion. This calculation loop was finally carried out for different work coefficients ($1 \leq \lambda \leq 1.8$). For every λ , three different mean diameters (90 mm, 95 mm and 100 mm) were chosen. This leads to different degrees of reaction, gearbox ratios, guide vane exit flow angles and circumferential velocities as shown in Tab. 5. A work coefficient of 1.1 results in a degree of reaction of ~ 0.5 . Since guide vanes and rotor blades can be designed in the same way with this configuration, these values have been chosen for the conversion. Furthermore, the gearbox with the lowest gearbox ratio was selected in favour of the lowest weight at $\lambda = 1.1$. Therefore, the mean diameter of the stage was thus set to 100

mm, what leads to a blade height of 12.5 mm and furthermore to an ITD-area ratio of $AR = 1.43$.

TABLE 5. POWER TURBINE DESIGN VARIANTS

λ [-]	d_m [mm]	i [-]	R_k [-]	α_8 [°]	n_{PT} [rpm]
1.0	90	12.6	0.55	40	63000
	95	11.9			59500
	100	11.3			56500
1.1	90	12.0	0.51	39.1	60000
	95	11.4			57000
	100	10.8			54000
1.2	90	11.5	0.46	38.4	57500
	95	10.9			54500
	100	10.4			52000
1.4	90	10.6	0.37	37.2	53000
	95	10.0			50000
	100	9.6			48000
1.6	90	9.9	0.27	36.4	49500
	95	9.4			47000
	100	8.9			44500
1.8	90	9.4	0.17	35.8	47000
	95	8.9			44500
	100	8.5			42500

Blade row

Based on the mean line analysis, a preliminary blade row was created. Therefore, adequate blade row parameters according to the calculated flow velocities and flow angles have to be chosen. These are basically stagger angle, chord to pitch ratio, leading edge- and trailing edge radius and wedge angles. First of all, a Zweifel coefficient Ψ was chosen, which describes the ratio of actual to maximum possible tangential aerodynamic force acting on the blade (8).

$$\Psi = 2 \left(\frac{t}{b} \right) \sin^2 \beta_9 (\cot \beta_8 - \cot \beta_9) \quad (8)$$

After that, an optimal axial chord to pitch ratio based on the obtained flow angles can be calculated according to [15]. To do this, Ψ was set to 1 at first. Common values lie in a range of $0.8 \leq \Psi \leq 1.2$, as Wilson and Korakianitis show [16]. They also give good guidelines for the calculation of preliminary design of

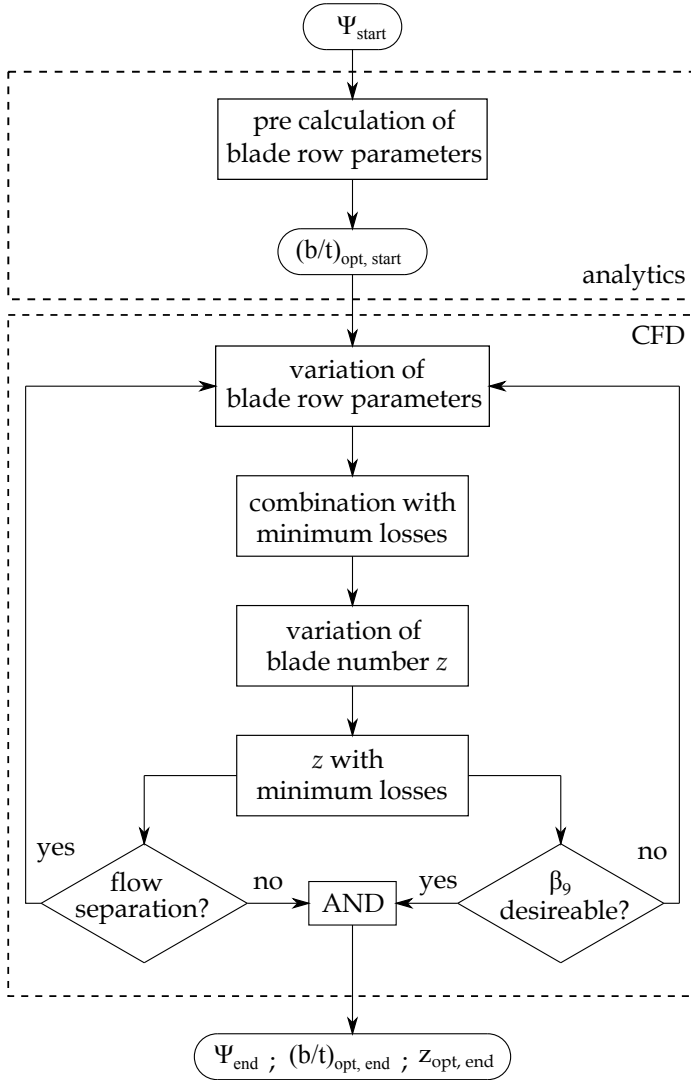


FIGURE 11. OPTIMAL BLADE NUMBER FLOW CHART

the blade profile and the selection of parameters which were used during this design. After a preliminary blade row was obtained, CFD simulations were used to improve the blade geometry in terms of minimizing losses. Therefore, different design points covering different combinations of blade row parameters have been investigated to find a configuration with minimal losses. The different design points were created automatically using optimal space filling method. The varied blade parameters are stagger angle, leading/trailing edge radius and wedge angles, throat width, throat angle and exit blade angle. As objective function, total pressure loss coefficient

$$\omega = \frac{\bar{p}_{t8} - \bar{p}_{t9}}{\bar{p}_{t9} - \bar{p}_9} \quad (9)$$

was chosen. The pressure values have been averaged by mass. Beside the blade row parameters, the number of blades z_B has been varied for a constant selected axial blade chord b . According to Eqn. (8), an optimal axial chord to pitch ratio can be obtained by changing the number of blades. For every variation of blade row parameters, the number of blades was changed between 27 (first obtained through Wilson method) and 60. Furthermore, it has to be checked, if the calculated flow field is free of flow separation and if the actual exit flow angle is in agreement with the calculated value from the mean line analysis (Fig. 11). Due to small blade heights, blades have been designed cylindrically.

CFD setup

The CFD calculations have been carried out with the commercial software ANSYS FLUENT 18.1 assuming steady-state, compressible flow with a relative inlet Mach number of $Ma_{w,1} = 0.42$, which was obtained previously through the analytical design. First of all, the blade row has therefore been designed with ANSYS DESIGN MODELER and the 3D mesh was created with ANSYS TURBO GRID, consisting of about 78000 cells per blade sector with $y^+ < 1$. Under the assumption of uniform inflow conditions, a sector model with periodic boundary conditions was used. Since compressible flow is supposed, total pressure at inlet and static pressure under consideration of radial equilibrium at the outlet have been used as boundary conditions. Due to the small dimensions, profile Reynolds number is in the order of $5 \cdot 10^4$. To cover turbulent effects, the SST $k-\omega$ turbulence model by Menter [17] including low Reynolds number correction has been used. The turbulent intensity has been set to 2% and a turbulent length scale of $0.01 \cdot t$ according to [18] was used at the inlet.

Results

Figure 12 shows the velocity field with streamlines of three different blade rows at mean section. Figure 12-(a) shows the initial blade row geometry which was obtained analytically. The number of blades was chosen for optimum chord to pitch ratio according to Eqn. (8) for $\Psi = 1$. The calculation results show a significant flow separation at the suction side due to low chord to pitch ratio and insufficient blade row parameters. Increasing number of blades, and consequently increasing the b/t ratio for this initial blade geometry shows, that minimum losses occur not at $b/t = 1.12$ as expected through calculation with the criteria of Zweifel according to Eqn. (8). It is suspected, that this is due to higher risk of flow separation at the suction side, when profile Reynolds number is low. Figure 12-(b) shows the streamlines at optimum blade number for an improved blade geometry. One can see, that the flow separation is now smaller in comparison to (a). For optimal blade number ($b/t = 1.41$), where ω is at a minimum for this geometry, Ψ takes a value of 0.79. This cor-

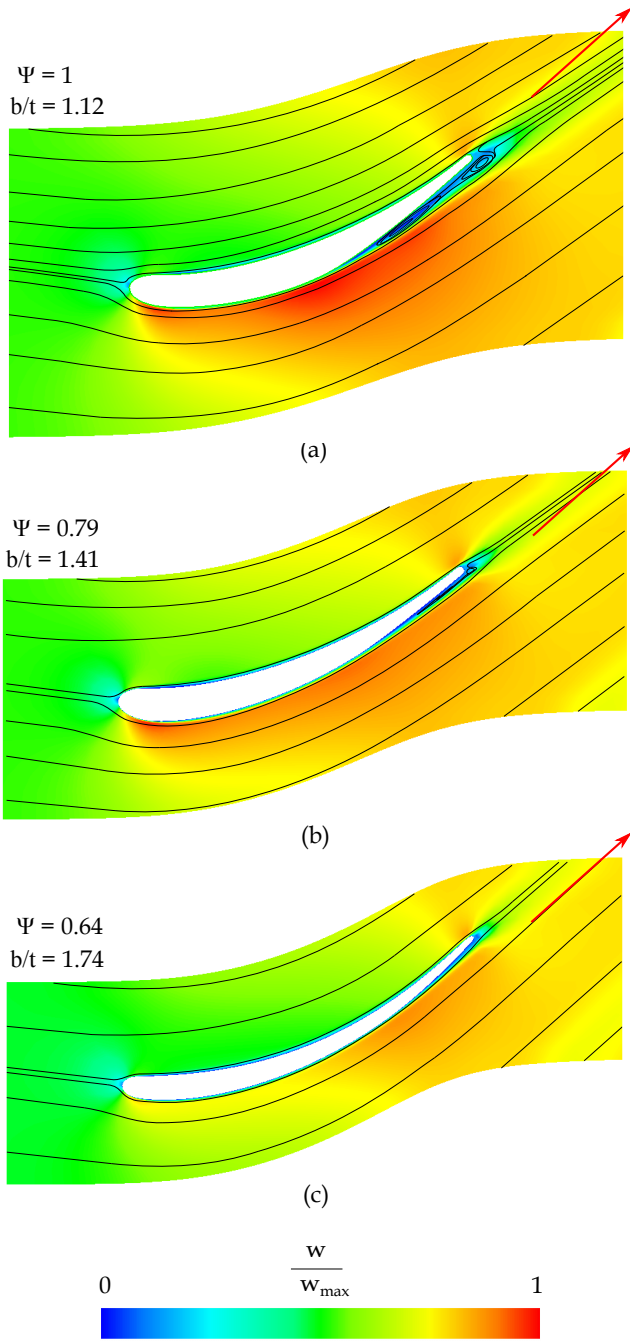


FIGURE 12. STREAMLINE-VELOCITY PLOT

responds very well to Zweifel, where optimum chord to pitch ratio takes a value of 1.40 for $\Psi = 0.8$ at given flow angles. Furthermore it can be seen, that the outflow angle β_0 meets not the required value for configuration (a) and (b). Figure 12-(c) shows the final preliminary blade row. Flow separation has now completely vanished and the exit flow angle corresponds well to the

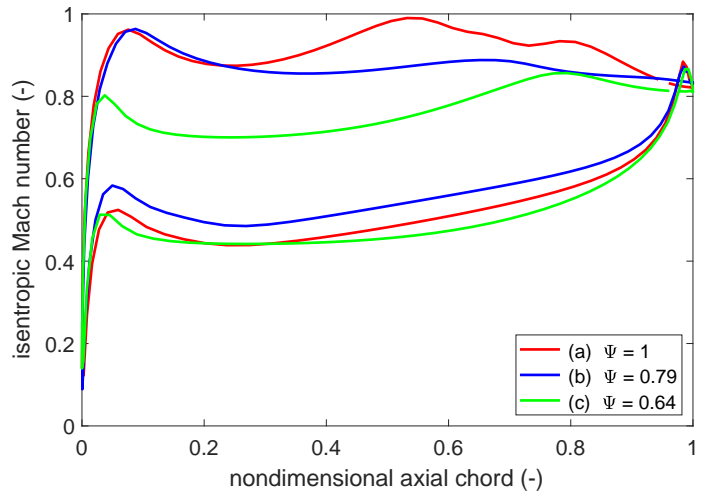


FIGURE 13. ISENTROPIC MACH NUMBER DISTRIBUTION

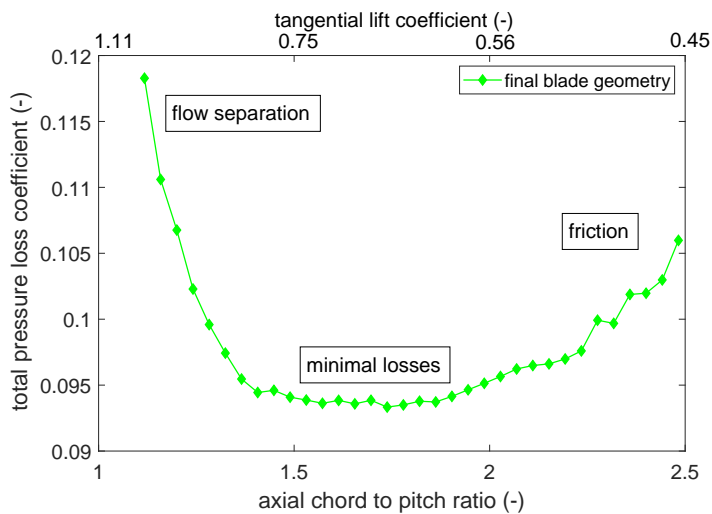


FIGURE 14. TOTAL PRESSURE LOSS

value gained through mean line analysis for the specified power output. The red arrow in Fig. 12 represents the desired exit flow direction. During the design process, one can see that the blade geometry becomes thinner as the process continues. Suction side curvature becomes more smooth towards configuration (c), what could be a further reason for the deviation of the Zweifel prediction for profile (a). Furthermore, the maximum velocity on the suction side is shifted towards the trailing edge.

The Mach number distributions over the blade surfaces are shown in Fig. 13. The distributions on the pressure side are widely similar for all cases because the pressure side geometry was hardly been changed. On the other hand, the suction side distribution shows a significant change during the improvement process. The initial blade row shows a highly fluctuating

distribution due to acceleration followed by flow separation due to deceleration. The improved blade row (b) shows a relatively constant distribution which is actually good. Nevertheless this design has to be modified because of poor exit flow conditions. For the final configuration, Fig. 14 shows the variation of total pressure loss coefficient as a function of chord to pitch ratio. The graph can be divided into three main areas. For few blades, high losses occur due to flow separation. With increasing number of blades, flow separation vanishes and losses are constant minimal for a relatively wide range. A further increase of blades lead to losses due to friction. It can be clearly seen, that losses are more influenced by flow separation than by friction due to a high gradient at low axial chord to pitch ratio. It is assumed that the present wide range of optimal axial chord to pitch ratio is due to the low deflection of the selected blade row. Due to the flat minimum, an optimal configuration can be found in a range between $0.6 \leq \Psi \leq 0.8$ at almost the same low losses. In terms of weight reduction and production effort, Ψ should be chosen as high as possible. Since the degree of reaction of the stage is about 0.5 and the blade geometry for the guide vane and rotor blade can be designed in the same way, the guide vane row is not considered in detail in this preliminary design.

CONCLUSIONS

In this work, a concept for micro-turbojet to micro-turboshaft engine conversion was presented. Through a first estimation, the amount of convertible shaft power could be obtained. Furthermore, a thermodynamic cycle model was developed considering effects due to the small dimensions. Since information of existing engines are usually rare, a recalculation of the gas generator of a chosen engine was presented to specify unknown boundary conditions. With a simultaneously carried out mean line analysis, unknown parameters e.g. component efficiencies could be estimated. After calculation of the boundary conditions, the design of the additional power turbine was presented. Therefore, an analytical preliminary design method also based on mean line analysis was shown. Additionally, a sufficient combination of mean diameter and work coefficient of the power turbine was found in terms of minimal gearbox weight. The calculations show, that minimum weight could be obtained using a work coefficient of 1.1 and a mean diameter of 100 mm under consideration of a favourable degree of reaction. The PT-power is about 50% of the GGT-power at a thermal efficiency of 13% and a specific fuel consumption of $180 \cdot 10^{-6}$ (kg/s)/kW. Furthermore, the blade row geometry was optimized using CFD calculations. Especially a range of optimum number of blades could be obtained changing axial chord to pitch ratio at a constant chord for a pre-optimized blade row. The optimum b/t ratio of 1.74 would lead to 42 blades. Decreasing the number of blades up to 34 would reduce manufacturing effort at nearly the same low losses. As a further research task, a structural analysis has to be done for

the gained blade geometry. An optimization of the ITD can also be a further topic of research in terms of minimizing losses and overall engine weight.

ACKNOWLEDGMENT

The authors would like to acknowledge the Austrian Research Promotion Agency FFG for supporting the project JET2SHAFT in the framework of the Aeronautics Research and Technology Programme TAKE OFF.

REFERENCES

- [1] Kadosh, K., and Cukurel, B., 2017. "Micro-Turbojet to Turbofan Conversion Via Continuously Variable Transmission: Thermodynamic Performance Study". *Journal of Engineering for Gas Turbines and Power*, **139**(2), February, p. 022603.
- [2] Elzahaby, A. M., Mohamed, K. K., and Badry, B. E., 2017. "Conversion of Turbojet Engine Jet Cat P200 to Turboprop Engine". *International Journal of Scientific and Engineering Research*, **8**(3), March, pp. 1447–1453.
- [3] Golchin, H., Ommi, F., and Saboohi, Z., 2019. *Assessment of converting approach of micro-turboprop engines*. CSAA - Chinese Journal of Aeronautics-<https://doi.org/10.1016/j.cja.2019.08.008>.
- [4] AMT Netherlands, 2018. *Olympus HP Specification*. URL <http://www.amtjets.com>.
- [5] Leylek, Z., Rowlinson, G., Anderson, W. S., and Smith, N., 2013. *An Investigation into Performance Modeling of a Small Gas Turbine Engine*. ASME Paper GT2013-94405.
- [6] Leylek, Z., 2012. *An Investigation into Performance Modeling of a Small Gas Turbine Engine*. Air Vehicles Division - Defence Science and Technology Organisation - Australian Government, DSTO-TR-2757.
- [7] Bakalis, D. P., and Stamatis, A. G., 2010. *Extended Instrumentation and Model Calibration for a Small Micro-Turbine*. ASME Paper GT2010-22837.
- [8] Rahman, N. U., and Whidborne, J. F., 2008. "A numerical investigation into the effect of engine bleed on performance of a single-spool turbojet engine". *Proceedings of the Institution of Mechanical Engineers, Part G: Journal of Aerospace Engineering*, **222**(7), July, pp. 939–949.
- [9] Vannoy, S., and Cadou, C. P., 2016. *Development and Validation of an NPSS Model of a Small Turbojet Engine*. 52nd AIAA/SAE/ASEE Joint Propulsion Conference - AIAA2016-5063.
- [10] Verstrate, T., Alsalihi, Z., and den Braembussche, R. A. V., 2006. *Numerical Study of the Heat Transfer in Micro Gas-turbines*. ASME Paper GT2006-90161.
- [11] Gong, Y., Sirakov, B. T., Epstein, A. H., and Tan, C. S.,

2004. *Aerothermodynamics of Micro-Turbomachinery*. ASME Paper GT2004-53877.
- [12] AMT Netherlands, 2018. *Internal pictures*. URL http://www.amtjets.com/internal_pics.php.
- [13] AMT Netherlands, 2019. *Re: Olympus HP in University configuration*. URL <http://www.amtjets.com>.
- [14] Rodgers, C., 1968. “A Cycle Analysis Technique for Small Gas Turbines”. *Proceeding of the Institution of Mechanical Engineers*, **183**(14), September, pp. 37–49.
- [15] Zweifel, O., 1945. *Die Frage der optimalen Schaufelteilung bei Beschaukelungen von Turbomaschinen, insbesondere bei grosser Umlenkung in den Schaufelreihen*. BBC-Mitteilungen.
- [16] Wilson, D. G., and Korakianitis, T., 1998. *The Design of High-Efficiency Turbomachinery and Gas Turbines*. Second edition, Prentice Hall.
- [17] Menter, F. R., 1994. “Two-Equation Eddy-Viscosity Turbulence Models for Engineering Applications”. *AIAA Journal*, **32**(8), August, pp. 1598–1605.
- [18] Hah, C., 1984. “A Navier-Stokes Analysis of Three-Dimensional Turbulent Flows Inside Turbine Blade Rows at Design and Off-Design Conditions”. *Journal of Engineering for Gas Turbines and Power*, **106**(2), April, pp. 421–429.